Output factor determination for dose measurements in axial and perpendicular planes using a silicon strip detector

Z. Abou-Haïdar,* A. Bocci, and M. A. G. Alvarez†

National Accelerator Center (CNA), 41092 Seville, Spain

J. M. Espino, M. I. Gallardo, M. A. Cortés-Giraldo, M. C. Ovejero, and J. M. Quesada

Department of Atomic, Molecular and Nuclear Physics (FAMN), University of Seville, 41012 Seville, Spain

R. Arráns

Virgin Macarena University Hospital, 41009 Seville, Spain

M. Ruiz Prieto

Faculty of Physics, University of Seville, 41012 Seville, Spain

A. Pérez Vega-Leal

School of Engineering, University of Seville, 41092 Seville, Spain

F. J. Pérez Nieto

Instalaciones Inabensa S.A., 41007 Seville, Spain

In this work we present the output factor measurements of a clinical linear accelerator using a silicon strip detector coupled to a new system for complex radiation therapy treatment verification. The objective of these measurements is to validate the system we built for treatment verification. The measurements were performed at the Virgin Macarena University Hospital in Seville. Irradiations were carried out with a Siemens ONCOR™ linac used to deliver radiotherapy treatment for cancer patients. The linac was operating in 6 MV photon mode; the different sizes of the fields were defined with the collimation system provided within the accelerator head. The output factor was measured with the silicon strip detector in two different layouts using two phantoms. In the first, the active area of the detector was placed perpendicular to the beam axis. In the second, the innovation consisted of a cylindrical phantom where the detector was placed in an axial plane with respect to the beam. The measured data were compared with data given by a commercial treatment planning system. Results were shown to be in a very good agreement between the compared set of data.

PACS numbers: 87.56.Fc, 87.55.km, 87.55.Qr

I. INTRODUCTION

For a given photon beam at a given source to surface distance (SSD), the dose rate at a certain depth d in a phantom depends on the field size. The output factor (OF) is defined as the ratio of the dose for any field size $A \times A$ cm^2 to the dose for a reference field at the same source to surface distance, and at the same depth d in a slab phantom. Usually the reference field is a square field of 10×10 cm^2 at an SSD of 100 cm; the larger the field size, the higher the dose [1]. The OF is an intrinsic characteristic of the accelerator and is measured periodically to make sure that the accelerator is operating properly in order to treat patients.

As mentioned above, in radiation therapy, the output factor is measured in slab phantoms. However, for the purpose of verifying our detection system and its calibration, we also measured the dose given by various square fields in an in-house designed cylindrical phantom normalized to the reference field, and we refer to it as output factor as well.

The measurements were carried out at the Virgin Macarena University Hospital in Seville. The accelerator is an electron linac (Fig. 1), Siemens ONCOR™ [2] dual energy machine used to deliver radiotherapy treatment for cancer patients. For our measurements it was operating in photon mode with a nominal energy of 6 MV. It is capable of generating high dose rate photons by colliding accelerated electrons on a tungsten target thus producing a bremsstrahlung effect. The different field sizes and shapes were

---

*ziadah@us.es

†Also at Department of Atomic, Molecular and Nuclear Physics (FAMN), University of Seville, 41012 Seville, Spain.

FIG. 1.   Experimental setup showing the accelerator's head where the collimating system is installed, and the cylindrical phantom described in Sec. II. The arrow shows the direction of the beam.

FIG. 2.   The slab phantom (left side) and the cylindrical rotating phantom (right side). The arrows show the direction of the beam.

obtained by using the collimation system provided within the accelerator head. It consists of a pair of jaws moving along the in-plane (longitudinal) direction and a multileaf collimator (MLC) moving along the cross-plane (transversal) direction. Longitudinal and transversal directions are related to the long and short dimensions of the treatment couch, respectively. The MLC incorporates 80 pairs of closely abutting tungsten leaves. Each leaf is individually motorized and controlled allowing the generation of irregular radiation fields [1]. In our case, rectangular and square fields were used.

The dose we are measuring is the dose deposited by the electrons that were accelerated by the photons hitting the phantom. The spectrum of these electrons depends on the field size. In Ref. [3] we have validated our system with a calibration using a reference field of 10×10 cm^2. In this work, we are testing our system by using it to measure the output factor in order to make sure that the same calibration is maintained while using different electron spectra associated to various field sizes and shapes.

In the experimental protocol section, we will expose the experimental setup as well as the materials and methods used for the experiment. In the discussion section, we will present the results obtained and compare them to other measurements performed using a waterproof air filled ionization chamber [4], manufactured by PTW, with an effective volume of 0.125 cm^3, and the treatment planning system (TPS—Philips Pinnacle^3) [5]. The TPS is a software that simulates the planned treatment strategies for every individual patient. However, it is highly advisable to verify complex plannings given by the TPS as it might miscalculate the delivered dose [3,6,7]. Finally, the conclusion section will summarize the measurements and the results obtained.

II. EXPERIMENTAL PROTOCOL

The detection system used combines a commercial W1(SS)-500 silicon detector from Micron Semiconductor

Ltd. [8] with an in-house developed setup based on two phantoms, electronics and data acquisition system [3].

A. The phantoms

The two phantoms (Fig. 2) that were designed to house the detector are briefly described below [3].

(i) A slab phantom made out of polyethylene ($30 \times 30 \times 2$ cm^3), where the detector's active area is placed perpendicular to the beam axis (Fig. 2, left side).

(ii) A polyethylene, cylindrical, rotating phantom (15 cm diameter and 17 cm length), used to simulate part of the human body in clinical conditions, where, as an innovation, the detector is placed in the axial plane, i.e., the active area of the detector is normal to the symmetry axis of the cylindrical phantom, and parallel to the beam axis (Fig. 2, right side).

The phantoms are designed to house the detector with a submillimetric precision. Then, the system is positioned on the treatment couch using the 1 mm thick laser provided in the room to position patients. The precision of the positioning of the phantoms is 1 mm, the same as for patients when using this same laser. Both phantoms were controlled by a slow control system, whose interface is developed on LABVIEW platform [9], for movement (in the case of the rotating phantom) and for data acquisition using the RS232 communication protocol [3].

B. The detector

The detector employed, shown in Fig. 3, is a commercial single sided silicon strip detector [model W1(SS)-500] from Micron Semiconductor Ltd. [8]. It is 500 μm thick with an active area of 50×50 mm^2, segmented on one side into 16 parallel strips, 3 mm wide each. The detector is an *n*-type silicon wafer, doped by acceptor impurities to create the 16 strips. Table I, provided by Micron Semiconductor Ltd., presents some characteristics of the detector.

C. Output factor in the slab phantom

For the slab phantom we considered an SSD of 100 cm, and a depth d of 1.5 cm. During the measurements, the slab phantom (Fig. 2, left side) was covered by 3 slabs of solid
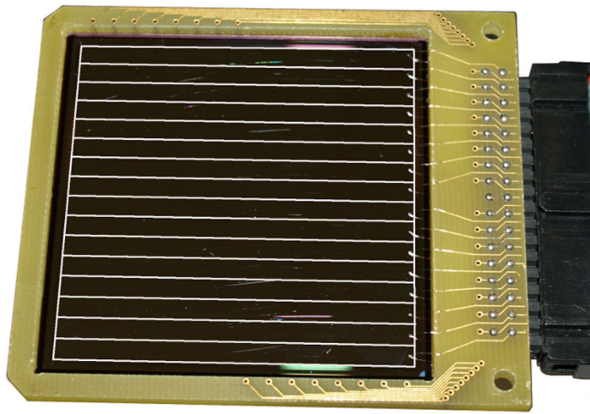
FIG. 3. W1(SS)-500 detector model from Micron Semiconductor Ltd. [8]; we can distinguish the 16 horizontal strips.
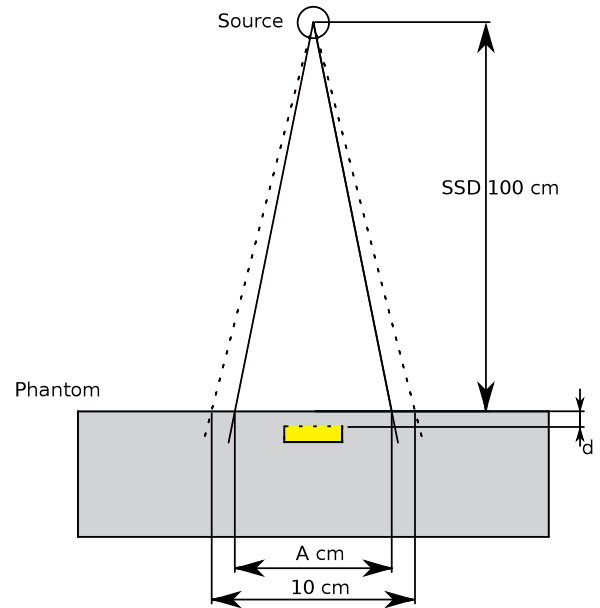

FIG. 4. Illustration of the output factor measurements in the slab phantom. The detector (rectangle inside the phantom) has its active area (indicated by dashed line) facing the source.

water of 0.5 cm thickness each. Figure 4 displays an illustration of the setup used for output factor measurements in the slab phantom. Dashed lines represent the reference field, and solid lines represent an $A \times A$ square field. For all output factor calculations in the slab phantom, we only considered dose received in the two central strips, 8 and 9. In a first set of measurements we used symmetric square fields centered in the center of the detector. Since the strip dimensions are 0.3×5 cm^2, we had to introduce a correction factor for fields smaller than 5×5 cm^2. This correction factor comes from the fact that to measure the dose, we have to integrate the absorbed energy not over the total area of the strip, but only over the irradiated area (i.e., area that is covered by the field). This factor could be obtained with the data from strips 1 to 16. However, since the aim of this work is not to measure the output factor as a final objective but to validate the detector calibration, TPS data are used as it provides higher precision. As an example, Fig. 5 represents the relative dose profile of the field 2×2 cm^2 given by the TPS.

Using the field profiles (Fig. 5), we performed an integration of each field considering all the dose contributions, including the tails of the profile, in order to calculate the equivalent size of the irradiation field.

Afterwards, the real dose corresponding to a field of $A \times A$ cm^2 ($A < 5$ cm) was obtained by measuring the energy deposited in the strip and dividing it by the equivalent irradiated volume [$v(A) \times 0.3 \times 0.05$ cm^3]; $v(A)$ being the integral, normalized to the unit, of the profile of the field $A \times A$ cm^2 including its tails. In fact, since our data acquisition software was configured to automatically divide the accumulated energy in each strip by the total strip volume ($5.0 \times 0.3 \times 0.05$ cm^3), we multiplied the obtained dose by 5.0 cm (length of a strip) and then divided it by the length corresponding to the irradiated part of the strip, which corresponds to the dimension of the field $v(A)$, hence the factor [$5/v(A)$].

In a second set of measurements we used rectangular fields of dimensions $A \times 3$ cm^2. The second dimension of the field (3 cm) was parallel to the strips. Since we were

TABLE I. Data sheet of the W1(SS)-500 detector provided by Micron Semiconductor Ltd. [8]

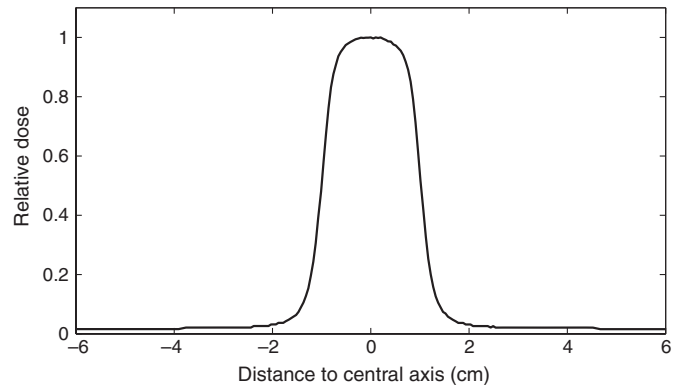| $N°$ junction elements:	16
Element length:	49.5 mm
Element pitch:	3.1 mm
Element width:	3000.0 μm
Active area:	50×50 mm^2
Thickness:	500 μm
Metallization:	Aluminum 0.3 μm
Package:	Printed circuit board with edge connections on one side

FIG. 5. Relative dose profile of the field 2×2 cm^2 given by the TPS [5].

TABLE II. Output factor in the slab phantom given by square fields. These data are represented in Fig. 9.

Field size (cm^2)	Output factor
2×2	0.793 ± 0.021
3×3	0.845 ± 0.017
4×4	0.834 ± 0.019
5×5	0.888 ± 0.023
5.6×5.6	0.932 ± 0.026
6×6	0.948 ± 0.024
7×7	0.972 ± 0.023
8×8	0.980 ± 0.025
9×9	0.992 ± 0.024
10×10	1.000 ± 0.000
15×15	1.027 ± 0.024

TABLE III. Output factor in the slab phantom given by rectangular fields. These data are represented in Fig. 10.

Field size (cm^2)	Output factor
1×3	0.808 ± 0.021
2×3	0.917 ± 0.030
3×3	0.954 ± 0.031
3.6×3	0.976 ± 0.021
4×3	0.973 ± 0.023
4.6×3	0.979 ± 0.021
5×3	0.986 ± 0.025
5.6×3	0.997 ± 0.019
6×3	0.993 ± 0.024
6.6×3	1.001 ± 0.024
7×3	0.992 ± 0.026
8×3	0.994 ± 0.019
9×3	1.000 ± 0.023
10×3	1.000 ± 0.000
15×3	1.005 ± 0.022
20×3	1.007 ± 0.020

comparing relative measurements and for simplifying the calculations, we used a normalization field of 10×3 cm^2.

Tables II and III represent the different fields measured in the slab phantom and their output factors associated. We considered an instrumental error of our in-house developed electronics of 0.65 cGy [3]. Moreover, by assuming that strips act as independent detectors, we calculated a statistical error by means of standard deviation. The cross talk between the strips was not taken into account, since, according to the fabricant, it is very small compared to the errors we calculated. Then, the error propagation method was applied to obtain the uncertainties for the output factor.

D. Output factor in the cylindrical phantom

As stated previously, in radiation therapy, the output factor is defined as the ratio of measured dose between a certain field and a reference field in a slab phantom perpendicular to the beam axis. However, in order to verify the viability of our detection system, we performed similar measurements for the cylindrical phantom with the detector parallel to the beam, and we also refer to them as output factor. In the cylindrical phantom that will be used for treatment verification setup, the detector is placed in the axial plane. We considered the SSD of 100 cm to be from the source to the center of the phantom. Figure 6 illustrates the experimental setup. We used square fields, and for each one of them we performed 19 measurements by rotating the phantom, hence changing the angle between the strips and the beam axis (Fig. 7) from $-90°$ to $+90°$ with steps of 10°. The detector is centered in the phantom, and the symmetry axis of the phantom coincides with the isocenter of the linac. The phantom was rotating around its symmetry axis. Afterwards, using an in-house developed algorithm based on the Radon transform [3,10], we reconstructed a 16×16 pixel dose map for each field. Each pixel is 3×3 mm^2. The output factor was then calculated considering the dose in the 4 central pixels. Figure 8 represents a reconstructed dose map for the 2×2 cm^2 field. In this figure, the only valid pixels are the ones contained inside the solid line circle. The black square in the center marks the 4 central pixels considered to calculate the output factor. Table IV displays the different measurements in the cylindrical phantom with their respective output factors.

For measurements in both the cylindrical and the slab phantom, as stated previously, we considered an instrumental error of our in-house developed electronics of 0.65 cGy [3]. Moreover, by assuming that strips act as
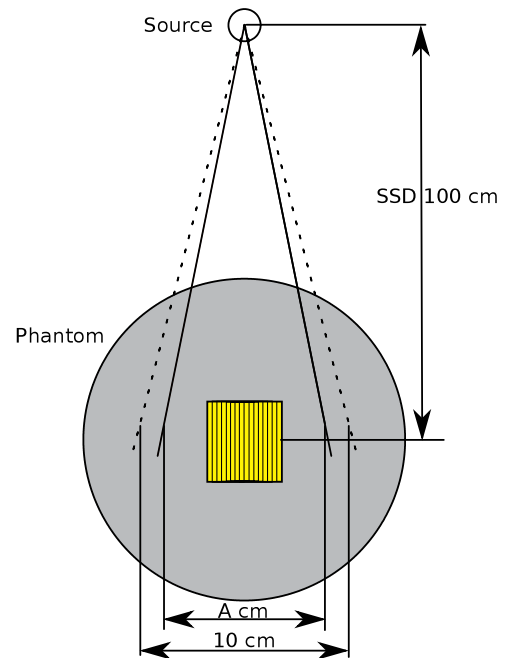

FIG. 6. Illustration of the output factor measurements in the cylindrical phantom. The segmented rectangle inside the phantom indicates the position of the detector's active area.
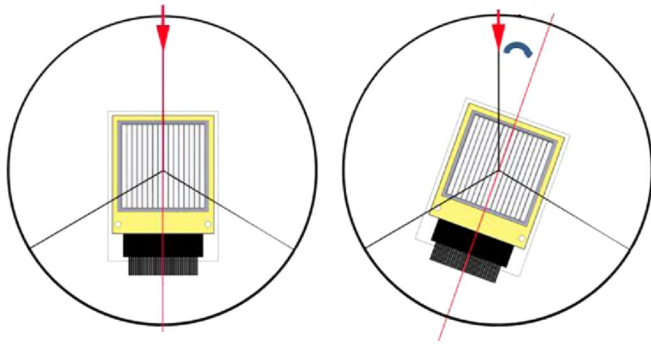
FIG. 7.   Illustration of the rotation of the detector and the angle between the strips and the beam axis (indicated by the arrow).
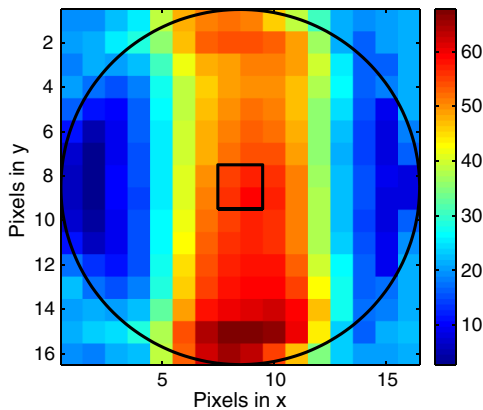

FIG. 8.   Reconstructed dose map for the 2×2 cm^2 in the cylindrical phantom. The legend on the right represents the dose value in cGy.

independent detectors, we calculated a statistical error by means of standard deviation. Data measured with the silicon detector [W1(SS)-500] will be compared with measurements performed with an ionization chamber or with TPS simulations [5] for which an error of 0.70 cGy in the dose was considered for fields bigger than 1×1 cm^2, and 1.20 cGy for fields of 1×1 cm^2. Then, the error propagation method was applied to obtain the uncertainties for the output factor.

TABLE IV.   Output factor in the cylindrical phantom given by square fields. These data are represented in Fig. 11.

Field size (cm^2)	Output factor
1×1	0.462 ± 0.007
2×2	0.766 ± 0.012
3×3	0.849 ± 0.013
4×4	0.897 ± 0.014
5×5	0.906 ± 0.014
6×6	0.916 ± 0.014
8×8	0.959 ± 0.014
10×10	1.000 ± 0.000
15×15	1.045 ± 0.016
20×20	1.064 ± 0.016

III. DISCUSSION

Figure 9 displays the results for the output factor for square fields in the slab phantom. Red filled circles represent the measurements with the silicon strip detector, and blue open squares represent the measurements with the ionization chamber.

Figure 10 shows the results for the output factor with rectangular fields in the slab phantom. Red filled circles represent the measurements with the silicon strip detector, and blue open squares represent the data given by the TPS [5] when implementing a virtual ionization chamber of 0.6 cm^3 volume.

In both cases, data are compatible within error bars. This shows the very good behavior of the silicon strip detector for output factor measurement.

Figure 11 represents the output factor measured in the cylindrical phantom. Red filled circles represent the measurements with the silicon strip detector, and blue open squares represent the data given by the TPS when implementing a virtual ionization chamber of 0.6 cm^3 volume. Data are also compatible as it is the case in the slab phantom, for fields bigger than 2×2 cm^2. However, for the 1×1 and 2×2 cm^2 fields, data are not compatible. This is provoked by the lack of electronic equilibrium [11] within the collecting volume of the detector occurring for small fields when the detector and the field are of a comparable size. Data for very small fields where points given by the silicon strip detector are below the ones given by the TPS are in agreement with results shown in Ref. [12] where the measured output factor decreases when increasing the size of the detector.

To summarize, the detector's calibration, which was performed with a field of 10×10 cm^2 [3], is still valid for other fields. However, for very small fields, we denote a larger difference due to a lack of electronic equilibrium since the strip size is comparable to the field size. In fact, in order to achieve electronic equilibrium, the detector should be very small compared to the field. This is not the case when measuring the dose of a 1×1 cm^2 field using a
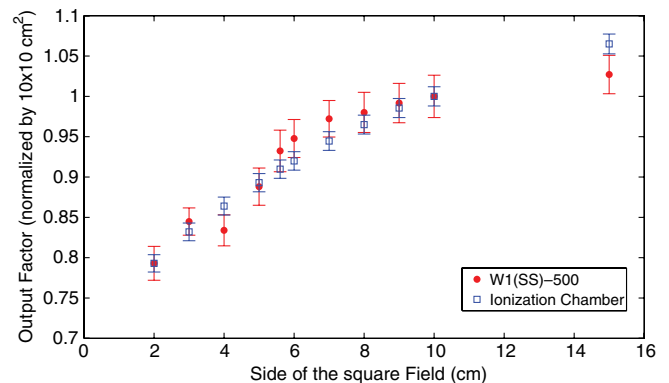

FIG. 9.   Output factor measured with different square fields in the slab phantom.
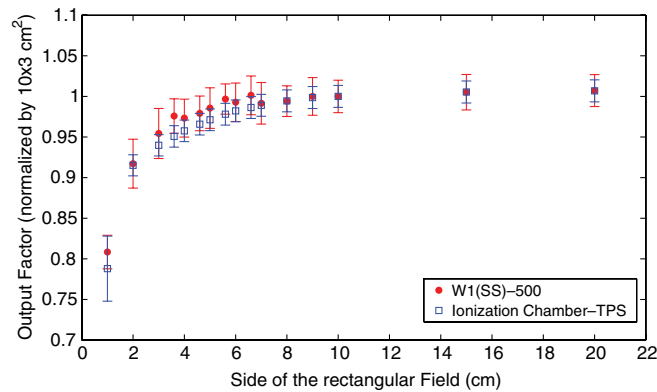
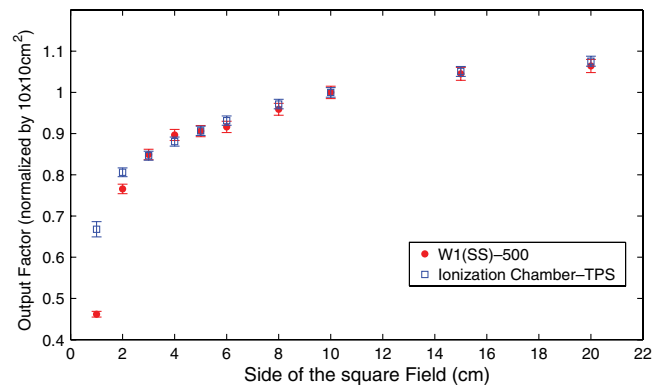FIG. 10.   Output factor measured with rectangular fields in the slab phantom.

FIG. 11.   Output factor measured with square fields in the cylindrical phantom.

6 mm width detection system (since we considered the two central strips to calculate the output factor). Up to a certain field size, performance of the detector is independent of the plane in which we are measuring and of the size of the field.

IV. CONCLUSIONS

This work is part of a more ambitious project aiming to develop a system dedicated to complex radiation therapy treatment verification in order to obtain online dose distribution [3,13]. In this paper we present output factor measurements of a Siemens ONCOR™ linac [2] performed with a silicon strip detector, model W1(SS)-500 from Micron Semiconductor Ltd. [8] coupled to in-house built phantoms, electronics, and slow control system.

Those measurements, performed for various field sizes and shapes, were compared to the ones carried out using the ionization chamber (either simulated with the TPS or experimentally measured), in order to validate the previously performed calibration of the system in standard conditions [3]. Each of Figs. 9–11 displays the compared sets of data. They present a remarkable agreement within the error bars as discussed in the previous section.

However, some differences were noted for very small fields due to dispersion and to the absence of electronic equilibrium [11].

As stated previously, the spectrum of the electrons set in movement by the photons entering the phantom depends on the field size. The change in the spectrum for different fields would come into play through its possible effect in the dose calibration of the detector, which would be reflected in the output factor. These measurements proved that this change is not relevant and that the calibration of the detector performed with a standard field (10×10 cm^2) is also valid for smaller ones that are usually employed for complex treatments. Once this has been validated, real treatments with any field size can be measured and dose maps could be obtained by an in-house Radon transform based algorithm [10]. Presently, research is in progress to achieve a larger active area detector (64×64 mm^2) including 2D strips with smaller strip pitch (2 mm), more precise electronics, an improved rotating phantom, and a user friendly data acquisition system.

[1] *Radiation Oncology Physics: A Handbook for Teachers and Students*, edited by E. B. Podgorsak (IAEA, Vienna, 2005) [http://www.iaea.org].
[2] "Siemens healthcare," available online at http://www.medical.siemens.com and http://www.medical.siemens.com/webapp/wcs/stores/servlet/CategoryDisplay~q_catalogId~e_-11~a_categoryId~e_1029068~a_catTree~e_100010,1008643,12757,1029071,1029068~a_langId~e_-11~a_storeId~e_10001.htm.
[3] A. Bocci, M. A. Cortés-Giraldo, M. I. Gallardo, J. M. Espino, R. Arráns, M. A. G. Alvarez, Z. Abou-Haïdar, J. M. Quesada, A. Pérez Vega-Leal, and F. J. Pérez Nieto, Nucl. Instrum. Methods Phys. Res., Sect. A **673**, 98 (2012).
[4] "Ptw," available online at http://www.ptw.de/semiflex_chambers0.html?cId=3475.
[5] "Philips healthcare," available online at http://www.healthcare.philips.com.
[6] J. Dyk, R. Barnett, J. Cygler, and P. Shragge, Int. J. Radiat. Oncol. Biol. Phys. **26**, 261 (1993).
[7] P. Cadman, R. Bassalow, N. Sidhu, G. Ibbott, and A. Nelson, Phys. Med. Biol. **47**, 3001 (2002).

[8] ''Micron Semiconductor Ltd., Solid State Detectors and Internet Solutions,'' available online at http://www .micronsemiconductor.co.uk/.

[9] ''National instruments,'' available online at http:// www.ni.com/labview/.

[10] M. I. Gallardo, M. A. G. Alvarez, J. M. Quesada, A. Pérez Vega-Leal, Z. Abou-Haïdar, A. Bocci, M. A. Cortés-Giraldo, J. M. Espino, R. Arráns, F. J. Pérez Nieto, and J. López-Domínguez, submitted for patent at the OEMP— Oficina Española de Patentes y Marcas—Ministry of Industry, Tourism and Commerce: Number P201101009 (13/09/2011).

[11] *The Physics of Radiology*, edited by H. E. Johns and J. R. Cunningham (Charles C Thomas Publisher Ltd., Springfield, IL, 1983).

[12] F. Sánchez-Doblado, G. H. Hartmann, J. Pena, J. V. Roselló, G. Russiello, and D. M. Gonzalez-Castaño, Physica Medica **23**, 58 (2007).

[13] M. A. Cortes-Giraldo, M. I. Gallardo, R. Arrans, J. M. Quesada, A. Bocci, J. M. Espino, Z. Abou-Haidar, and M. A. G. Alvarez, Prog. Nucl. Sci. Technol. **2**, 191 (2011) [http://www.aesj.or.jp/publication/pnst002/data/ 191-196.pdf].